Final Project Report

Dynamics of Groundwater and Surface Water Related to the Mangrove/Marsh Ecotone

Dr. James E. Saiers
Principal Investigator
Yale University
205 Prospect Street
New Haven, CT 06511

USGS Cooperative Agreement No. 01ERAG0066

Background

The research supported under this cooperative agreement was aimed at advancing current understanding of the hydrology of the coastal mangrove ecosystem and the adjacent freshwater marsh of Everglades National Park. The specific objectives of this study were to (1) quantify hydrologic properties that govern the flow of groundwater and surface water and (2) construct models appropriate for describing the movement of water and waterborne constituents in surface and subsurface environments.

This two-year project has led to the publication of three peer-reviewed journal articles, one appearing in the *Journal of Hydrology* [Bolster and Saiers, 2002. 259:221-235] and two appearing in *Groundwater* [Bolster, Genereux, and Saiers, 2001. 39:768-777; Saiers, Genereux, and Bolster, in press]. The manuscript published in the *Journal of Hydrology* describes the development and testing of a mathematical model appropriate for describing transient surface-water flow in Shark River Slough. The manuscripts appearing in *Groundwater* center on estimation of hydrogeologic properties of the portion of the Biscayne Aquifer beneath Everglades National Park.

This cooperative agreement also supported the examination of factors that govern the transport of particulate matter within the surface waters of Shark River Slough. This research, which was carried out in collaboration with Judson Harvey (USGS, Reston), integrated mathematical modeling with field-scale experimentation. The field experiment involved injecting particles composed of TiO_2 into surface water and monitoring their transport as they moved through the emergent vegetation under natural-gradient conditions. We developed a three-dimensional mathematical model and used it quantify the coupled mass transport and mass-transfer processes that governed particle transport in the field experiment. The tracer experiment on particle transport is the first of its kind, and our analysis of this experiment provides new

knowledge critical for addressing a broad range of issues related to tree-island evolution, seed and larval dispersal, and contaminant migration.

The second year of the project focused primarily on the execution, analysis, and interpretation of the particle-transport experiment. The remainder of this annual report describes these three aspects of the study.

Site Description

The particle tracer experiment was performed at a surface-water flume facility constructed in Shark River Slough, which is an elongate, low-lying zone that delivers freshwater from the Water Conservation Areas along the northern boundary of Everglades National Park to Whitewater Bay and the Gulf of Mexico. The flume facility, maintained and operated by researchers at Florida International University, has four side-by-side channels, each 3.25 m wide and extending for 100 m in a southerly direction. (Noe et al. [2002] provides details on the construction of the flume facility.) Our experiment was conducted in the westernmost channel on 21 November 2002, when the depth of water in the channel equaled 60 cm. Calcium and bicarbonate were the principal ionic species in surface-water samples collected from the channel. This water contained high concentrations of dissolved organic carbon (14 mg/L) and had a pH and ionic strength of 6.9 and 0.007 M, respectively. *Eleocharis cellulose* (806 stems/m^2) and *Eleocharis elongata* (341 stems/m^2) composed the dominant macrophytes in the channel, and periphyton (a matrix of algae and heterotrophic microbes) persisted as a discontinuous mat floating on the top few centimeters of the water column and as thin coatings ("sweaters") on macrophyte stems. The macrophytes were anchored in peat, which was approximately 0.5 m in thickness and underlain by limestone.

Experimental Methodology

Particles composed of titanium dioxide (TiO_2) were suspended in filtered (0.2 μM) Everglades water and used as the tracer. Background concentrations of TiO_2 in Shark River Slough are exceedingly low, so the TiO_2 tracer particles could be distinguished from the autochthonous particles on the basis of their chemical signature (see below). The mean zeta potential of the TiO_2 particles, calculated from electrophoretic mobility measurements, equaled -20 mV, and the average particle size, determined by photon correlation spectroscopy, equaled 0.3 μM.

We introduced a 9 g/L TiO_2 suspension 0.75 m upgradient of the leading edge of the vegetation, which is located approximately 10 m from the head of the channel (Figure 1A). The injection was accomplished by using a metering pump to deliver the TiO_2 tracer at constant rate (100 ml/min) through a slotted hose that was emplaced 24 cm below the water surface and that spanned the central 1.95 m of the channel (Figure 1B). The duration of the injection was 0.9 hours. Sampling for the TiO_2 began before the start of the injection and continued for 3 hours after termination of the injection. Water samples (20 mL) were repeatedly collected in plastic scintillation vials by applying suction to stainless steel minipiezometers installed at discrete points located 7.5 m down channel from the injection (Figures 1A and 1B). The minipiezometers are designated as LS, LM, LD, CM, RS, RM, and RD, where L (left), C (center), and R (right) delineate lateral position and refer to locations 0.9 m inside the left wall, at the channel center, and 0.9 m inside the right wall, respectively, and S (shallow), M (mid-depth), and D (deep) delineate vertical position and refer to depths of 0.148, 0.273, and 0.423 m, respectively.

Concentrations of titanium (Ti) in the water samples were measured in the laboratory following dissolution of the TiO_2 particles. Two milliliters of concentrated, ultra-pure HNO_3

(Seastar) were added to 10 mL aliquots of the field samples, and the acidified samples were placed on a shaker table facilitate particle dissolution. The samples were removed from the shaker table after 12 hours, diluted 1:1 with Nanopure water, and analyzed for Ti concentrations by inductively coupled plasma mass spectrometry (ICP-MS, Thermo Finnigan Element 2). Analysis of acidified standard suspensions of known TiO_2 concentration indicated that titanium recoveries exceeded 97% for Ti concentrations between 1 μg/L and 5 mg/L.

Mathematical Model

We quantified particle advection, dispersion, and immobilization kinetics by comparing measured TiO_2 breakthrough curves to those calculated by a mathematical model. The model solves an equation that accounts for coupled advective-dispersive transport and rate-limited mass transfer in a domain of constant water depth, where particle dispersion is anisotropic and the mean flow velocity is uniform (i.e., independent of position) and in the direction parallel to the x axis of the coordinate system:

$$\frac{\partial C}{\partial t} = \frac{\partial}{\partial x}\left[D_{Lon}\frac{\partial C}{\partial x}\right] + \frac{\partial}{\partial y}\left[D_{Lat}\frac{\partial C}{\partial y}\right] + \frac{\partial}{\partial z}\left[D_{V}\frac{\partial C}{\partial z}\right] - V\frac{\partial C}{\partial x} - ?C \qquad (1)$$

where C is the surface-water concentration of particles, D_{Lon}, D_{Lat}, and D_V are the longitudinal, lateral, and vertical dispersion coefficients, respectively, V is the mean surface-water velocity, and λ is a mass transfer coefficient for particle immobilization. Interception by aquatic vegetation and adsorption of particles that diffuse to the sediment were among the plausible mechanisms of particle immobilization in our experiment; however, sedimentation did not contribute significantly to TiO_2 removal because the settling velocity of these particles is very small ($< 10^{-2}$ cm/h).

We employed a finite-element method to solve equation (1) for a three-dimensional domain measuring 10 m long, 3.25 m wide (the channel width), and 0.6 m deep (Figure 1A).

The numerical solution was obtained for zero initial TiO_2 concentrations, a zero-gradient in TiO_2 concentrations across the lateral boundaries (i.e., advective flux >> dispersive flux), and zero total flux across both the free surface and ground surface. A specified TiO_2 flux along a planar internal boundary (0.05 m X 1.95 m) was used to simulate the injection source (Figures 1A and 1B).

Observations from a separate experiment on the transport of bromide (a conservative tracer) revealed that the channel walls were permeable and that a significant cross-channel component of surface-water flow existed. While the bromide data could not be used to make quantitative determinations about surface-water flow during the TiO_2 experiment (because the magnitude of flow velocities varied between experiments), the bromide results did emphasize the need to account for cross-channel flow within our modeling framework. We accomplished this by computing the magnitude and direction of the mean surface-water velocity from the component velocities and then we rotated the coordinate system for the model domain such that the x axis was parallel with the direction of V. The magnitude and direction of the mean surface-water velocity is expressed by

$$V = (v_1^2 + v_2^2)^{1/2} \qquad (2)$$

and

$$\Theta = \tan^{-1}(v_1/v_2) \qquad (3)$$

where v_1 and v_2 are the components of the surface-water velocity parallel to the channel wall and perpendicular to the channel wall, respectively (Figure 1A).

We applied the model in inverse mode in order to estimate v_1 and v_2, as well as the parameters that govern dispersion (D_{Lon}, D_{Lat}, and D_V) and particle-immobilization kinetics (λ). Best-fit values of the model parameters were identified by using a Levenberg-Marquardt

algorithm to minimize and objective function, defined as the sum-of-the-squared residuals between model-calculated concentrations and those measured in samples collected from the minipiezometers.

Results

Model Sensitivity Analysis

We examined the sensitivity of particle breakthrough at the minipiezometer positions to changes in the parameters that govern advection, dispersion, and particle immobilization kinetics. This involved comparing a simulation generated with a base-case set of parameter values to modeled results obtained by individually adjusting ?, D_V, and v_2 from their base-case values of

2 h^{-1}, 0.005 m^2 h^{-1}, and 0 m h^{-1}, respectively.

Model calculations made with the base-case parameters reveal that particle concentrations for the sampling-site positions on the left side of the channel (i.e., LS, LM, LD) are identical to those computed for corresponding depths on the right side (i.e., RS, RM, RD) (Figure 2A). Three conditions combine to produce this symmetry in particle breakthrough: the left- and right-side sampling sites are spaced equal distances from the channel center, the injection source is centered laterally within the channel, and the flow field parallels the channel walls (i.e.,$V=v_1$ and $\Theta=90^?$). Peak breakthrough concentrations at the mid-depth samplers are greatest at the central sampling point (CM) and decrease towards the left (LM) and right (RM) owing to dilution by lateral dispersion. On both the left and right sides of the channel, breakthrough concentrations decline with vertical distance away from the injection source (see Figure 1B for sampler depths); that is, concentrations at the mid-depth samplers (LM and RM) are higher than concentrations at the shallow samplers (LS and RS), which are, in turn, are higher than those at the deep samplers (LD and RD) (Figure 2A).

Variation in the value of ? controls the magnitude of the breakthrough concentrations. An increase in the mass-transfer coefficient from 2 h^{-1} to 3 h^{-1} leads to a 3-fold decline in breakthrough concentrations (compare Figures 2A and 2B). Changes in ? do not affect the apparent dispersion or travel time of the suspended particles, however. Because the immobilization rate varies linearly with C, increases in ? promote proportionate reductions in breakthrough concentrations at all minipiezometers.

The model-simulated breakthrough curves exhibit pronounced sensitivity to adjustments in the dispersion coefficients. D_V regulates the distribution in particle concentrations between the mid-depth sampling sites and the shallow and deep sampling sites. Vertical mixing decreases as D_V declines from its base case value to 0.001 m^2 h^{-1}, so the particles (which were injected near mid depth) do not spread in appreciable concentrations to the shallow and deep sampling sites, and particle transport is relegated to the middle of the water column, leading to comparatively higher breakthrough concentrations at the mid-depth samplers (compare Figures 2A and 2C)

We adjusted v_2 from its base case value of zero in order to explore the effects of cross-channel flow on particle breakthrough. For v_2 = -2 m/h (the negative sign signifies that cross-channel component of flow is from right to left), symmetry in particle breakthrough between the left and right sampling sites disappears and concentrations on the left side of the channel grow at the expense of concentrations on the right side of the channel (compare Figures 2A and 2D). Cross-channel flow also lowers peak breakthrough concentrations because particles exit the channel before being detected at the monitoring points.

Comparison of Field Observations and Model Calculations

TiO_2 particles appeared at the sampling sites approximately one hour after the injection was initiated. Measured breakthrough concentrations were highest at the mid-depth samplers and, among these samplers, the magnitude of the breakthrough decreased from the left side of the

channel (LM), where concentrations peaked at 57 µg/L to the right side of the channel (RM), where concentrations peaked at 5 µg/L (Figure 3). Concentrations did not exceed background levels at either deep sampler or at the right-side shallow sampler, but breakthrough was clearly apparent at LS.

Calculations of the advection-dispersion model match the measured breakthrough data reasonably well (Figure 3), though deviation between experimental and modeled results exists. The largest discrepancy is associated with CM, where the model overpredicts the maximum concentrations by 29%. Apart from this discrepancy, the model captures the range in observed breakthrough behavior, from the near-zero concentration at the deep samplers to the high concentrations recorded at LM.

We conducted the inverse simulation with different starting values for the adjustable parameters. In each case, the model converged to the same parameter values. Correlation between fitted parameters is low, ranging from 0.11 to 0.75, and the standard errors of the parameter estimates do not exceed 7.6% of the corresponding parameter value. These least-squares regression statistics suggest that the inverse solution is unique and that the field data are sufficient to precisely estimate the model parameters [*Hill et al.*, 1998].

The best-fit values of v_1 and v_2 are 6.1 and -2.0 m/h, respectively, which corresponds to a mean surface-water velocity (V) of 6.3 m/h. As shown by the sensitivity-analysis results, the cross-channel component of flow, signaled by the non-zero value of v_2, leads to the asymmetry in breakthrough concentrations between the left and right sides of the channel. Dispersion of the TiO_2 particles was small. The best-fit values of the longitudinal dispersion coefficient (D_{Lon}) and the lateral dispersion coefficient (D_{Lat}) were nearly equal at 0.25 and 0.24 $m^2\ h^{-1}$, respectively, and 250 times greater than the vertical dispersion coefficient ($D_V = 0.001\ m^2\ h^{-1}$).

The small D_z is consistent with our observations that the TiO_2 plume traveled through the center of the water column and did not spread appreciably to the shallow and deep samplers.

Immobilization rates were fast, with the optimal value of λ equaling 3.2 h^{-1}. Based on this estimate, the time scale for particle immobilization (λ^{-1}) is 0.3 hours, which is approximately 4 times less than time required for the particles to be transported by advection from the line-source injection to the array of minipiezometers. The absence of tailing on the experimental breakthrough curves suggests that particle immobilization can, according to our assumptions, be considered an irreversible process, at least on the time scale of our experiment.

Discussion

The mean surface-water velocity estimated from our experiment is 6.3 m h^{-1}, which, for the average stem diameter measured within the channel (0.2 cm), corresponds to a stem Reynolds Numbers (Re_s = Vd/?, where ? is the kinematic viscosity and d is stem diameter) of approximately 3. This value is more than an order of magnitude less than Re_s values reported for studies conducted with dissolved tracers in tidal marshes or in laboratory flumes containing model vegetation [*Leonard and Luther*, 1995; *Nepf et al.*, 1997] and indicates that flow velocities in our experiment were too small to generate turbulence within stem wakes. Given that stem wakes dominate turbulence production in wetland environments [*Nepf*, 1999], these results imply that turbulent mixing of the TiO_2 particles was insignificant.

For the low-Re_s flow observed in this study, the stem-wake structure is laminar and particle-spreading rates reflect contributions of Brownian diffusion, bed-induced shear, and mechanical dispersion. Brownian diffusion played a negligible role in dispersive mixing within the channel, as the Brownian diffusion coefficient for the TiO_2 particles (= 5 X 10^{-9} m^2/h) is several orders of magnitude lower than the best-fit estimates of D_{Lon}, D_{Lat}, and D_V. Like Brownian diffusion, boundary-induced shear flow was not an important contributor to particle

dispersion, because, within aquatic vegetation, gradients in velocity attributable to retardation of flow near the bed surface are restricted to a narrow region (i.e., 1 – 2 cm) adjacent to the bed [*Nepf*, 1997]. This boundary layer lies well below the portion of the water column sampled by the TiO_2 tracer cloud. Mechanical dispersion, or mixing caused by local variations in the direction and velocity of flow around the mean velocity (V), represented the dominant mechanism of TiO_2-particle dispersal. The local variations in advective transport that promote mechanical dispersion are not caused by turbulence, but arise from small-scale heterogeneity in the density of vegetation and resulting nonuniformities in flow resistance and tortuosity of particle-transport pathways.

Comparison of the modeled and measured breakthrough concentrations demonstrate that mechanical dispersion is anisotropic, with spreading in the longitudinal and lateral directions exceeding dispersion in the vertical direction by more than two orders of magnitude. The comparatively small vertical dispersion is consistent with observations of solute transport through geologic environments [*Gelhar et al.*, 1992], which, like wetland systems, are composed of tortuous transport pathways, and suggests that vertical variation in vegetative structure is considerably less than that in the horizontal directions. These results also indicate that vertical mixing of particles is exceedingly slow in the absence of strong winds or other conditions that could promote turbulence. In our experiment, where the water depth (h) equaled 0.6 m, the time scale for complete vertical mixing ($= h^2/D_V$) was 360 h.

Model calculations made with the best-fit parameter values show that peak breakthrough concentrations were 60 times lower than those calculated assuming conservative advective-dispersive transport (i.e., $\lambda = 0$). The TiO_2 particles were too small to be susceptible to removal by settling (see section 4), and the particles did not diffuse to the bottom of the channel, where

they would be susceptible to removal by adsorption to the bed sediments. There is also no evidence to support particle trapping with stagnation zones as a significant particle removal mechanism because breakthrough-curve tailing, a diagnostic feature of this reversible mass-transfer process, was not observed in our experiment. Interception of particles by aquatic vegetation, in particular by *Eleocharis cellulose* and *Eleocharis elongata*, represented the primary mechanism of particle removal within the surface-water channel.

The effectiveness of the plant stems in scavenging TiO_2 from the water column can be quantified in terms of a single-stem collection efficiency (η_S), which expresses the ratio that particles stick to a single stem to the rate that particles approach a single stem from upstream. Particles are removed from a unit volume of surface water at the rate λC and thus are collected by (stick to) a single stem at the rate $?C\left(\frac{h}{P}-\frac{phd^2}{4}\right)$, where P is the stem density (stems/m^2) and the quantity in parentheses is the volume of water associated with a single (cylindrical) emergent stem of diameter d. The rate at which particles approach the stem is $VChd$, giving

$$?_S = \frac{?_w}{dV}\left[\frac{1}{P}-\frac{pd^2}{4}\right] \quad (4)$$

The η_s value computed with the best-fit estimates of λ and V and with measurements of P (= 1150 stems/m^2) equals 0.2, indicating that a single stem is capable of scavenging 20% of the particles that approach its projected cross-sectional area from the upstream direction. We suspect this high stem-collection efficiency is due, in part, to periphyton sweaters that coat the plant stems and provide a substrate favorable for particle attachment. While we have not positively identified the properties that make vegetation efficient particle collectors, this analysis does illustrate that mass-transfer reactions with emergent vegetation strongly affect the

concentrations of waterborne particulate matter and must be accounted for in quantitative predictions of particle transport.

References

Gelhar, L.W., C. Welty, and K.R. Rehfeldt, A critical review of data on field-scale dispersion in aquifers, *Water Resources Research*, *28*, 1955-1974, 1992.

Hill, M.C., R.L. Cooley, and D.W. Pollock, A controlled experiment in ground water model calibration, *Ground Water*, *36*, 520-535, 1998.

Leonard, L.A. and M.E. Luther, Flow hydrodynamics in tidal marsh canopies, *Limnology and Oceanography*, *40*, 1474-1484, 1995.

Nepf, H.M., The effects of vegetation on longitudinal dispersion, *Estuarine, Coastal and Shelf Science*, *44*, 675-684, 1997.

Nepf, H.M., Drag, turbulence, and diffusion in flow through emergent vegetation, *Water Resources Research*, *35*, 479-489, 1999.

Nepf, H.M., J.A. Sullivan, and R.A. Zavistoski, A model for diffusion within emergent vegetation, *Limnology and Oceanography*, *42*, 1735-1745, 1997.

Noe, G.B., D.L. Childers, A.L. Edwards, E. Gaiser, K. Jayachandran, D. Lee, J. Meeder, J. Richards, L.J. Scinto, J.C. Trexler, and R.D. Jones, Short-term changes in phosphorus storage in an oligotrophic Everglades wetland ecosystem receiving experimental nutrient enrichment, *Biogeochemistry*, *59* (3), 239-267, 2002.

Figure Legends

Figure 1. (A) Plan-view positions of the tracer injection source and minipiezometers within the portion of the channel used for the particle-tracer experiment. The model domain, measuring 10 m long and 3.25 m wide, is situated near the head of the 100-m long channel. (B) Cross-sectional positions of the tracer-injection source and minipiezometers as viewed from the head of the channel.

Figure 2. Model-calculated TiO_2 breakthrough curves for (A) base-case parameter values, (B) $\lambda = 3\ h^{-1}$, (C) DV = 0.001 $m^2\ h^{-1}$, and (D) v2 = -2 m h^{-1}. The breakthrough curves are referenced by the lateral and vertical positions of the minipiezometers (see Figure 1B). In D, only breakthrough curves calculated for the mid-depth minipiezometers are shown.

Figure 3. Measured (symbols) and modeled (lines) breakthrough concentrations of TiO_2. Measured and modeled TiO_2 concentrations at LD, RS, and RD remained at baseline levels during the injection and are not shown.

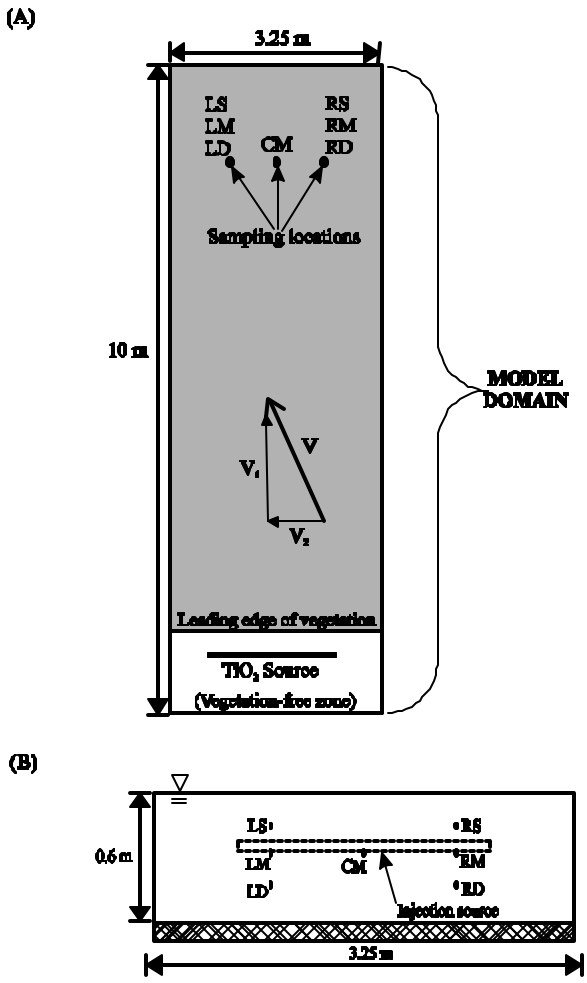
(A)
3.25 m
LS
LM
LD
CM
RS
RM
RD
Sampling locations
10 m
MODEL DOMAIN
V
V1
V2
Leading edge of vegetation
TiO2 Source
(Vegetation-free zone)
(B)
0.6 m
LS
LM
LD
CM
RS
RM
RD
Injection source
3.25 m

Figure 1.

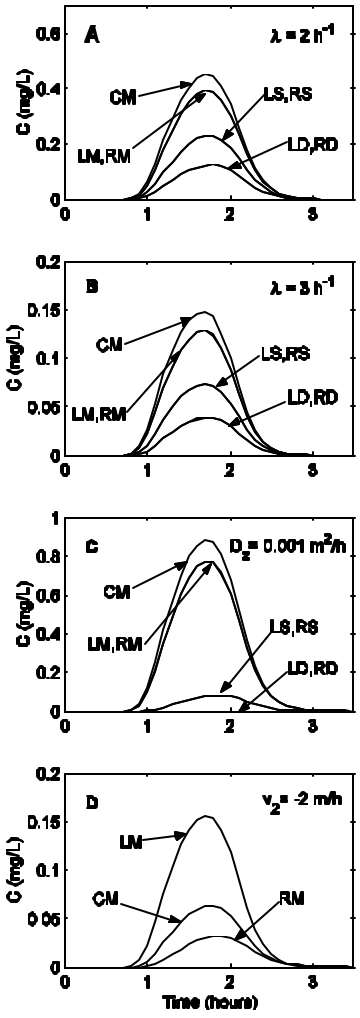
A
λ = 2 h-1
C (mg/L)
CM
LS,RS
LM,RM
LD,RD
B
λ = 3 h-1
C
D2= 0.001 m2/h
D
v2= -2 m/h
LM
RM
Time (hours)

Figure 2.

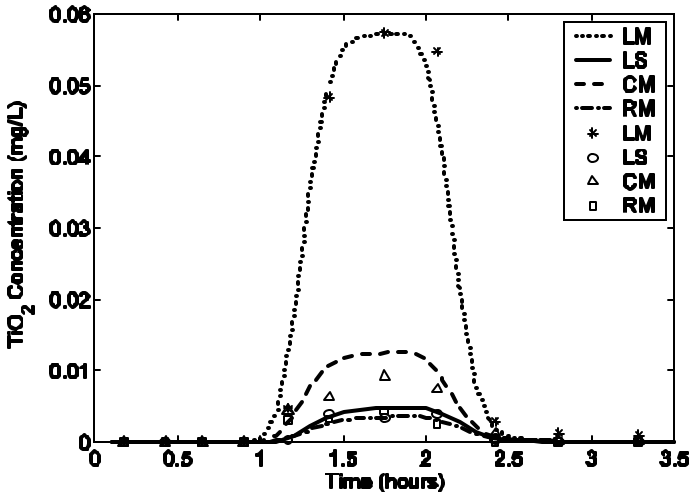
0.06
0.05
0.04
0.03
0.02
0.01
0
TiO2 Concentration (mg/L)
0
0.5
1
1.5
2
2.5
3
3.5
Time (hours)
LM
LS
CM
RM
LM
LS
CM
RM

Figure 3.